

Nd elastic scattering as a tool to probe properties of 3N forces

H. Witała¹, W. Glöckle², J. Golak^{1,2}, A. Nogga², H. Kamada^{2*}, R. Skibiński¹,
J. Kuroś-Żołnierczuk¹.

¹*Institute of Physics, Jagellonian University, PL-30059 Cracow, Poland*

²*Institut für Theoretische Physik II, Ruhr Universität Bochum, D-44780 Bochum, Germany*
(November 3, 2018)

Abstract

Faddeev equations for elastic Nd scattering have been solved using modern NN forces combined with the Tucson-Melbourne two-pion exchange three-nucleon force, with a modification thereof closer to chiral symmetry and the Urbana IX three-nucleon force. Theoretical predictions for the differential cross section and several spin observables using NN forces only and NN forces combined with three-nucleon force models are compared to each other and to the existing data. A wide range of energies from 3 to 200 MeV is covered. Especially at the higher energies striking three-nucleon force effects are found, some of which are supported by the still rare set of data, some are in conflict with data and thus very likely point to defects in those three-nucleon force models.

21.30.-x, 21.45.+v, 25.10.+s, 24.70.+s

Typeset using REVTeX

*present address: Institut für Strahlen- und Kernphysik der Universität Bonn Nussallee 14-16, D53115 Bonn, Germany

I. INTRODUCTION

One major goal in nuclear physics is to establish the properties of nuclear forces and to understand nuclear phenomena by solving the many- nucleon Schrödinger equation driven by those elementary nuclear forces. Meson theory had an important impact for the construction of nuclear forces (both NN and 3N forces), but it lacks systematics like it would be given by an expansion parameter and the meson-nucleon vertices had to be parametrised in an ad-hoc manner. Nevertheless the one-pion exchange is undisputed and the most advanced formulation of meson-exchanges in the so called full Bonn potential [1] is remarkably successful. Because of its energy dependence - a consequence of deriving it by old fashioned time ordered perturbation theory - it is not useful in $A > 2$ systems. Energy independent one-boson exchange versions thereof, however, are useful [2,3]. In addition more phenomenological NN potentials have been constructed with the aim to describe the rich set of experimental NN data as precisely as possible. This leads to an often called new generation of realistic NN potentials: AV18 [4], CD Bonn [5], Nijm I, II and 93 [3]. They describe the NN data set with an unprecedented precision of χ^2 per data point very close to one. Very recently an updated CD Bonn [6] appeared, which takes newest data into account but has not been used in the present article. An upcoming approach to construct nuclear forces in a systematic manner is chiral perturbation theory [7–13]. First applications to three- and four-nucleon systems have been done [14].

In recent years it became possible to solve exactly three- and four-nucleon bound states using standard integration and differentiation methods [15,16]. Stochastic techniques allow to go beyond $A=4$ and right now low energy states of nuclei up to $A=8$ are under control [17,18]. In all cases those realistic NN forces fail to provide the experimental binding energies; there is clear cut underbinding. For instance this amounts to 0.5-1 MeV in case of three nucleons and to 2-4 MeV in case of ${}^4\text{He}$. A natural further step is the consideration of 3N forces. This is an even harder theoretical challenge and presently the most often used dynamical process is the $\pi - \pi$ exchange between three nucleons with an intermediate excited nucleon state, the Δ [19]. This is augmented by further ingredients of various types as will be detailed below. By properly adjusting parameters one can achieve correct 3N and 4N binding energies and reaches even a fairly successful description of low energy bound states energies of up to $A= 8$ [20]. However, in the latter case the results point to an insufficient spin-orbit splitting of nuclear levels in light nuclei as e.g. in ${}^5\text{He}$ [17]. This may be caused by a wrong spin structure of present day 3NF's or by not well enough established 3P_j NN force components. It will be interesting to see in the future the predictions of nuclear forces based on chiral perturbation theory.

Though this first signal on 3N force effects resulting from discrete states is important, a more detailed investigation of 3NF properties can be carried through in scattering processes, where a rich set of spin observables is available. The tremendous advance in computational resources allowed in recent years to make exact predictions for three- nucleon scattering using nuclear forces in all their complexities [21]. Also experimentally one can access nowadays spin observables in Nd scattering where in the initial states the deuteron and / or the nucleon is polarized and after the reaction also the polarization of the outgoing particles can be measured [22,24–30]. This leads to a very rich spectrum of observables in Nd elastic scattering and the Nd break-up processes. Such a set of spin observables will be a solid basis

to test the 3N Hamiltonian. Using available model Hamiltonians one can provide guidance in selecting specific observables and energies which are most appropriate to see 3NF properties. It is the aim of this article to do exactly that and to compare the theoretical predictions with already existing data.

In section II we review briefly our 3N scattering formalism and display the 3NF model forces which are presently en vogue and which we use. Some technical details referring to the partial wave decomposition of the momentum space representation of the Urbana IX 3NF [31] are given in the Appendix. In this article we restrict ourselves to elastic Nd scattering and refer to a forthcoming article for the break-up process. Our predictions for various nuclear force combinations and the comparison to available data are given in section III. We conclude in section IV.

II. SCATTERING FORMALISM AND 3NF MODELS

We refer to [21] for a general overview on 3N scattering and specifically our way to formulate it. For the inclusion of 3NFs we found meanwhile a more efficient way [32]. It is a direct generalization of what is being used for the 3N bound state [33]. We define an amplitude T via our central equation

$$T = tP\phi + (1 + tG_0)V_4^{(1)}(1 + P)\phi + tPG_0T + (1 + tG_0)V_4^{(1)}(1 + P)G_0T \quad (1)$$

The initial channel state ϕ occurring in the driving terms is composed of a deuteron and a momentum eigenstate of the projectile nucleon. The NN t -operator is denoted by t , the free 3N propagator by G_0 and P is the sum of a cyclical and an anticyclical permutation of three particles. The 3N force V_4 can always be decomposed into a sum of three parts

$$V_4 = V_4^{(1)} + V_4^{(2)} + V_4^{(3)}, \quad (2)$$

where $V_4^{(i)}$ is symmetrical under the exchange of the nucleons jk with $j \neq i \neq k$. As seen in Eq. (1) only one of the three parts occurs explicitly, the others via the permutations contained in P . The physical break-up amplitude is given via

$$U_0 = (1 + P)T. \quad (3)$$

The Faddeev-like integral equation (1) has the nice property that its iteration inserted into Eq. (3) yields immediately the multiple scattering series, which gives a transparent insight into the reaction mechanism. Here in this article we concentrate on elastic scattering, whose amplitude is given by

$$U = PG_0^{-1} + PT + V_4^{(1)}(1 + P)\phi + V_4^{(1)}(1 + P)G_0T \quad (4)$$

The first term is the well known single particle exchange diagram, then there are terms where either V_4 or the t 's interact once and then the remaining parts result from rescattering among the three particles. Again inserting the iteration of T as given in Eq. (1) into Eq. (4) yields a transparent insight [34].

The definition of the various spin observables can be found in [21,35]. They have the general form

$$\langle S^\mu \rangle_f I = \frac{1}{6} \sum_\nu \langle S^\nu \rangle_i \text{Tr} (M S^\nu M^\dagger S^\mu), \quad (5)$$

where I is the elastic cross section summed over the spin states in the final state, M is the physical elastic scattering amplitude related directly to U and S^μ is a suitable set of 3N spin operators.

We shall encounter nucleon and deuteron vector analyzing powers $A_y(N)$ and $A_y(d)$ (iT_{11}), where in the initial state either the nucleon (N) or the deuteron (d) is vector polarized. Further, the deuteron can be tensor polarized in the initial state leading to the three tensor analyzing powers T_{2k} ($k = 0,1,2$). Also both particles can be polarized in the initial state leading to very many spin correlation coefficients $C_{\alpha,\beta}$, where α refers to the spin directions of the nucleon and beta to vector and tensor polarizations of the deuteron. Further information on the dynamics can be found in spin transfer coefficients $K_\alpha^{\beta'}$, where α describes either a polarized nucleon or a polarized deuteron in the initial state and β' similarly the polarization for a particle in the final state. Of course all those quantities depend on the scattering angle.

Our nuclear model interaction consists of one of the NN forces mentioned in the introduction and a 3NF. For the 3NF we use the 2π -exchange Tucson Melbourne (TM) model, a modified version thereof and the Urbana IX force. The TM model [36] has been around for quite some time. It is based on a low momentum expansion of the $\pi - N$ off (the- mass) shell scattering amplitude. It has the form [36]

$$V_4^{(1)} = \frac{1}{(2\pi)^6} \frac{g_{\pi NN}^2}{4m_N^2} \frac{\vec{\sigma}_2 \cdot \vec{Q}}{\vec{Q}^2 + m_\pi^2} \frac{\vec{\sigma}_3 \cdot \vec{Q}'}{\vec{Q}'^2 + m_\pi^2} H(\vec{Q}^2) H(\vec{Q}'^2) \left\{ \vec{\tau}_2 \cdot \vec{\tau}_3 \left(a + b\vec{Q} \cdot \vec{Q}' + c(\vec{Q}^2 + \vec{Q}'^2) \right) + di \vec{\tau}_3 \times \vec{\tau}_2 \cdot \vec{\tau}_1 \vec{\sigma}_1 \cdot \vec{Q} \times \vec{Q}' \right\}. \quad (6)$$

The elements of the underlying Feynman diagram are obvious: the two pion propagators depending on the pion momenta \vec{Q} and \vec{Q}' , the two πNN vertex amplitudes and most importantly the parametrisation of the πN amplitude inside the curly bracket which is combined with the isospins $\vec{\tau}_2$ and $\vec{\tau}_3$ of the two accompanying nucleons. On top of all that there is a strong form factor parametrisation given by

$$H(\vec{Q}^2) = \left(\frac{\Lambda^2 - m_\pi^2}{\Lambda^2 + \vec{Q}^2} \right)^2 \quad (7)$$

In what we denote by the TM 3NF we use the original parameters $a = 1.13/m_\pi$, $b = -2.58/m_\pi^3$, $c = 1.0/m_\pi^3$, $d = -0.753/m_\pi^3$. They incorporate among others the physics resulting from an intermediate Δ in a static approximation. The cut-off parameter Λ is used to adjust the 3H binding energy separately for different NN forces [37]. For the convenience of the reader we show the Λ -values in Table 1. Of course in a meson exchange picture additional processes should be added containing other meson exchanges like $\pi - \rho$, $\rho - \rho$; also different intermediate excited states might play a role. To some extent 3NF models with respect to those extensions have already been developed and applied [38–41]. Further studies should be performed.

The parametrisation of the TM 3NF has been criticized somewhat, since it violates chiral symmetry [42,43]. A form consistent with chiral symmetry (though not a complete

one to that order in the appropriate power counting) is obtained by modifying the c -term so that the long-range part is absorbed into the a -term, leading to a new $a' \equiv a - 2m_\pi^2 c = -0.87/m_\pi$ [42,43] what essentially means a change of sign for a and that the short range part is dropped. This form will be called TM' later on. The corresponding Λ -value when used with the CD Bonn potential is $\Lambda = 4.593 m_\pi$.

The two-meson exchange 3NF has also been studied by Robilotta *et al.* [44] leading to the Brazilian 3NF. It is similar to the one of TM and also the results gained for low energy Nd elastic scattering observables [45] are similar to the ones for the TM 3NF. In this article we do not take that force into account. Instead we included the Urbana IX 3NF [31], which is heavily used in the Urbana-Argonne collaboration. It will be interesting to see its effects for 3N scattering observables. At very low energies it has been used in that context before by the Pisa group [46]. That force is based on the old Fujita-Mijazawa ansatz [47] of an intermediate Δ occurring in the two-pion exchange and augmented by a spin independent short range piece. It has the form

$$V_4^{(1)} = A_{2\pi} \left[\{X_{12}, X_{13}\} \{\vec{\tau}_1 \cdot \vec{\tau}_2, \vec{\tau}_1 \cdot \vec{\tau}_3\} + \frac{1}{4} [X_{12}, X_{13}] [\vec{\tau}_1 \cdot \vec{\tau}_2, \vec{\tau}_1 \cdot \vec{\tau}_3] \right] + U_0 T_\pi^2(r_{12}) T_\pi^2(r_{13}), \quad (8)$$

where

$$X_{ij} = Y_\pi(r_{ij}) \vec{\sigma}_i \cdot \vec{\sigma}_j + T_\pi(r_{ij}) S_{ij}, \quad (9)$$

with

$$Y_\pi(r) = \frac{e^{-m_\pi r}}{m_\pi r} (1 - e^{-cr^2}), \quad (10)$$

and

$$T_\pi(r) = \left[1 + \frac{3}{m_\pi r} + \frac{3}{(m_\pi r)^2} \right] \frac{e^{-m_\pi r}}{m_\pi r} (1 - e^{-cr^2})^2, \quad (11)$$

and where

$$S_{ij} = 3 \vec{\sigma}_i \cdot \hat{r}_{ij} \vec{\sigma}_j \cdot \hat{r}_{ij} - \vec{\sigma}_i \cdot \vec{\sigma}_j \quad (12)$$

is the tensor operator.

Since we work in momentum space and in a partial wave expansion the form given in Eq. (8) has to be rewritten. We could follow the steps laid out before for the corresponding representation of the TM 3NF [48] and delegate all that to the Appendix.

Since there is no apparent consistency of the mostly phenomenological realistic NN forces and the 3NF models we test various combinations thereof. In all cases, however, we require that the particular choice for the 2N interaction and the 3NF should reproduce the experimental triton binding energy. Some of the 3N observables scale with the triton binding energy [49]. The adjustment to the triton binding energy has the advantage that our investigation is not misled by these scaling effects.

With respect to the intermediate Δ one should say that very likely the static approximation is not justified and the Δ should be allowed to propagate like the nucleon. This has been pursued intensively for instance by the Hannover group [50] and recent work has been also devoted to the 3N continuum [51].

In view of all that it is quite clear that our present study is not at all complete but can at most provide some insight, what kind of effects specific 3NF models might generate. As we shall see effects of that sort are needed, since NN force only predictions often fail to describe the data, especially at the higher energies. These challenges call for a systematic approach and at least for the leading spin structures chiral perturbation theory might be a good candidate [8]. This is left to a future investigation. Here we concentrate on the current models and show their strengths and failures.

III. PREDICTIONS OF 3NF EFFECTS AND COMPARISON TO DATA

Since we would like to cover a wide range of incoming neutron energies from below the nd breakup threshold up to 200 MeV it is necessary to take a sufficient number of partial wave states into account in order to get converged solutions of the Faddeev equations. In all calculations presented in this paper we went up to the two-nucleon subsystem total angular momentum $j_{max} = 5$. This corresponds to a maximal number of 142 partial wave states (often called channels) in the 3N system. We checked that the convergence has been achieved by looking at the results obtained for $j_{max} = 6$, which increases the number of channels to 194. This convergence check refers to a calculation without a 3NF. The inclusion of 3NF's has been carried through for all total angular momenta of the 3N system up to $J = 13/2$. These high angular momenta are required at the higher energies ≥ 100 MeV. The longer ranged 2N interactions require states up to $J = 25/2$ at the higher energies in order to get converged results.

A phenomenological criterium for 3NF effects is that the data lie outside the spread of NN force predictions only. In the following figures we shall always include a shaded band (called “band1”), which covers the predictions of the AV18, CD-Bonn, NijmI, II and 93 NN forces. Unfortunately we cannot include the pp-Coulomb force in our approach and thus have to live with some theoretical uncertainty when comparing to pd-data. At the higher energies, however, those effects should be small. Also in case of AV18 we do not take the various electromagnetic corrections into account, which leads for example to a slightly wrong deuteron binding energy ($E_d = 2.242$ instead of 2.225 MeV). This, however, has only a small effect on our results, which is mostly of kinematical origin, since the phase-shifts obtained without those additional terms differ only slightly from the standard ones. The kinematical effects are seen predominantly in the breakup process, where this small defect in the deuteron binding energy leads to correspondingly small shifts in peak structures like for instance final state interaction peaks.

We shall combine another group of curves into a band. The TM 3NF can be combined with the five NN forces. In all cases the cut-off value Λ in Eq. (7) has been adjusted separately for each NN force to the ${}^3\text{H}$ binding energy [37]. Since that interplay is a purely phenomenological step the outcome is theoretically not under control and we combine all the results into a second band (called “band2” in the following). Next we want to compare the TM 3NF and the modified TM', which is more consistent with chiral symmetry. We combine

it with CD-Bonn and show the CD-Bonn+TM' prediction as a dashed curve. Finally we compare the TM and the Urbana IX 3NF's and combine them with AV18. The combination AV18+URBANA IX will appear as a solid curve. There are clearly more combinations possible but it is sufficient to get an orientation on the magnitudes of expected effects.

We begin with the differential cross section in Fig. 1. The various NN force predictions are rather close together with a small spread in the minima. Including the TM 3NF there is again a small spread in the minima (practically negligible at 3 MeV) but the minima are shifted upwards, rather well into the data [52] except at 3 MeV, where the 3NF prediction is shifted slightly downwards. The phenomenon of shrinkage of the spread between different NN potential predictions by including a 3NF is often called a scaling phenomenon. It occurs at low energies and is related to the three-nucleon binding energy, which by construction is common to all those curves in band2. The TM and TM' 3NF's together with CD-Bonn give slightly different predictions in the minima especially at the two highest energies. (The CD Bonn+TM prediction lying inside band2 is not shown.) In the backward angular region they differ significantly and the 135 MeV precise backward angular distributions data prefer the TM 3NF. (See insertion in Fig. 1; again the CD Bonn+TM prediction is not explicitly shown.) On the other hand TM and URBANA IX together with AV18 are very similar at the two higher energies but differ significantly at $E=65$ MeV. Certainly Coulomb force effects should be taken into account at this energy before a final conclusion can be drawn. The few nd data near the minimum would strongly disagree with all our 3NF predictions and a confirmation (or rejection) would be highly desirable. However, independent from possible Coulomb force contributions, it is clearly seen, that even such a simple observable as the elastic scattering differential cross section exhibits large 3NF effects at higher energies. These effects are not trivial and depend not only on the incoming energy and the angle but also on the particular 3NF used. This calls for precise data for this observable in order to study the 3NF properties.

Let us now regard a selection out of the many spin observables in elastic Nd scattering. Fig.2 shows $A_y(N)$. The band for NN force predictions is always rather narrow, whereas band2 for the lowest and highest energy is distinctly broader. The two bands are separated predicting clearly 3NF effects especially at higher energies. The TM and TM' predictions are distinctly different as well as the TM and Urbana IX predictions. It is interesting to note that here TM' with CD Bonn and Urbana IX with AV18 are very similar (except at the lowest energy) and predict only small 3NF effects at 65 MeV, which are compatible with the A_y data at this energy. At higher energies their effects become quite different from the TM ones. While in the region of the A_y minimum around $\theta_{cm} \approx 110^\circ$ they increase A_y as compared to the pure 2N force predictions, their action decreases A_y in the backward angular region, contrary to the action of the TM 3NF model, bringing the theory closer to the data. In this way the TM' and Urbana IX 3NF's seem to solve partially the A_y problem found at higher energies in [27,53]. At 3 MeV the clear discrepancy of all theoretical predictions to the nd data of [54] is seen. At such a low energy it is well known that Coulomb force effects are large for A_y decreasing significantly its maximum when compared to nd data [55]. Thus also pd data lie very clearly (due to much smaller error bars) above all theoretical predictions. We see that this very well known low energy A_y puzzle [56] cannot be solved by the 3NF models we are using in this article. A slightly increased maximum of A_y for TM' is far too small to play any significant role and possibly the solution should be also sought in an

improvement of the 3P_j NN force components [57] to which low energy A_y is very sensitive. We would also like to point to the very recent result based on chiral perturbation theory [14], where A_y can be described quite well in next-to-leading order (NLO). In that order of the power counting 3NF's do not yet contribute. Those effective chiral NN forces are very different from the conventional ones. But this NLO result is just an intermediate step and the final answer has to wait for higher order contributions, which improve systematically the observables in the 2N, 3N, ... systems at the same time.

For iT_{11} shown in Fig. 3 the two bands are distinctly different and clearly the TM-band is supported by the data at the higher energies. In that case TM and TM' are close together and also TM and URBANA IX except around 120° at the highest energy. The data shown in the figure for 190 MeV are taken at 197 MeV. Unfortunately they are absent around 120° .

Next we regard the three tensor analyzing powers T_{20} , T_{21} and T_{22} in Figs. 4-6. For T_{20} the situation is very challenging. At 135 MeV the data between about 120° - 150° do not agree with the overlapping bands and above 150° they lie just between the two bands. At small angles they agree with the overlapping bands and follow then the NN force prediction. In addition at the higher energies TM and TM' differ as well as TM and URBANA IX. The strong deviations of the theory to the data at 3 MeV is simply caused by Coulomb force effects [58].

For T_{21} the situation is different. The two bands are clearly distinct. Again the different 3NF's predictions deviate strongly from each other. The data at 135 MeV follow more band1 than band2 and at the small angles TM' or URBANA IX are preferred. Clearly this is a rather contradictory situation.

For T_{22} the bands differ but the special 3NF predictions (dashed and solid lines) are similar but lie outside band2. Except at very backward and forward angles, where all curves essentially coincide, there is disagreement with the data at $E=135$ MeV. For all three T_{2k} 's data at 190 MeV would be very valuable, since the various theoretical predictions differ dramatically.

There are many spin-transfer coefficients and we selected more or less arbitrarily five of them. In Figs. 7-11 we show $K_{yz}^{x'}$, $K_{yy}^{y'}$, $K_{xx}^{y'}$, $K_{xz}^{y'}$ and $K_x^{y'z'}$. For $K_{yz}^{x'}$ the bands strongly deviate at the higher energies and TM and TM' as well as TM and URBANA IX differ drastically. The deviation of the bands from each other is less pronounced for $K_{yy}^{y'}$ and also the different 3NF predictions are less distinct except at the highest energy. Two data points agree with the 3NF predictions, while one, at 150° , is below any theoretical prediction. For $K_{xx}^{y'}$ the bands differ only at the lowest energy ($E=3$ MeV) significantly. Otherwise the 3NF effects are rather modest and also differences among the different 3NF's. The data at 135 MeV go across the various predictions. For $K_{xz}^{y'}$ the bands differ at the high energies and the two special 3NF predictions deviate significantly from the TM predictions. The one data point at 135 MeV lies somewhere in between. Finally $K_x^{y'z'}$ show again dramatic effects in relation to the two different bands. Also the special 3NF predictions are clearly different at the two higher energies.

Lastly we regard in Figs. 12-14 three different spin correlation coefficients $C_{xy,x}$, C_{yy} and C_{zz} . The effects are dramatic for $C_{xy,x}$: the bands are quite different and also the special 3NF predictions. For C_{yy} there are data [26] at $E_p = 197$ MeV, which we inserted into the figure for 190 MeV. The data support the curves inside band2. The AV18+URBANA IX

is significantly closer to experiment than CD Bonn+TM'. Finally for C_{zz} the bands differ a lot at the high energies and the special 3NF predictions differ from the TM ones as well. One notes that URBANA IX and TM' are similar.

IV. SUMMARY AND CONCLUSIONS

We performed a study of popular present day 3NF models with respect to the effects they cause in the 3N continuum. Based on the comparison of the realistic NN force predictions alone (“band1”) to the predictions of all NN forces combined with the TM 3NF (“band2”) one sees in many spin observables very drastic effects, which should clearly be discernible by experiments. On top the three different 3NF models, TM, TM' and URBANA IX combined (arbitrarily) with CD-Bonn and AV18 lead again to other very distinct predictions. Specifically the effects are angular and energy dependent becoming large at higher energies. It seems that with a sufficiently rich and precise data basis such diversity of effects should allow to nail down the proper spin structure of 3NF's.

Unfortunately there are up to now only few data available. The ones for the differential cross section support the shift in theory caused by 3NF's. The existing high energy cross section data in the backward angular region prefer the structure of the TM 3NF. Also the existing deuteron vector analyzing powers at higher energies support rather well the predicted 3NF effects. On the other hand this three-body interaction predicts too large effects for the nucleon analyzing power. This observable seems to prefer the modified version of the Tucson-Melbourne model, TM', which is consistent with chiral symmetry or the URBANA IX. For the tensor analyzing powers the situation is totally chaotic, for some scenarios one finds agreement, for others a strong disagreement: there is no preference for any of them. Clearly we are at the very beginning in investigating the spin-structure of the 3NF. Nevertheless the effects of all those 3NF's are typically of the right order in magnitude, when they can be checked against data but the signs are not yet under control. The spin transfer coefficients carry also a lot of information and in some of them the two bands differ very much. Finally, the spin correlation coefficients appear also very informative and the very first data for C_{yy} support the TM and URBANA IX.

Altogether the only conclusion possible is that the most popular current 3NF models show a lot of effects and data are needed to provide constraints. There is hope that further theoretical work guided by the chiral effective field theory approach will help to establish the proper spin structure of the three-nucleon force.

ACKNOWLEDGMENTS

This work was supported by the Deutsche Forschungsgemeinschaft (H.K., A.N. and J.G.), the Polish Committee for Scientific Research under Grant No. 2P03B02818 and the Science and Technology Cooperation Germany-Poland. W.G. would like to thank the Foundation for Polish Science for the financial support during his stay in Cracow. The numerical calculations have been performed on the Cray T90 and T3E of the NIC in Jülich, Germany.

APPENDIX A: PARTIAL WAVE DECOMPOSITION OF THE URBANA IX 3NF IN MOMENTUM SPACE.

The Urbana 3NF in Eq.(8) has to be put into a form suitable for the evaluation in partial wave decomposition. Therefore we rewrite Eq.(8) using the (anti)commutator of the isospin operators

$$\begin{aligned}\{\vec{\tau}_1 \cdot \vec{\tau}_2, \vec{\tau}_1 \cdot \vec{\tau}_3\} &= 2 \vec{\tau}_2 \cdot \vec{\tau}_3 \\ [\vec{\tau}_1 \cdot \vec{\tau}_2, \vec{\tau}_1 \cdot \vec{\tau}_3] &= 2i \vec{\tau}_1 \cdot \vec{\tau}_2 \times \vec{\tau}_3\end{aligned}\tag{A1}$$

$V_4^{(1)}$ reads then

$$\begin{aligned}V_4^{(1)} &= A_{2\pi} 2 \left(\vec{\tau}_2 \cdot \vec{\tau}_3 + \frac{i}{4} \vec{\tau}_1 \cdot \vec{\tau}_2 \times \vec{\tau}_3 \right) X_{12} X_{13} \\ &\quad + A_{2\pi} 2 \left(\vec{\tau}_2 \cdot \vec{\tau}_3 - \frac{i}{4} \vec{\tau}_1 \cdot \vec{\tau}_2 \times \vec{\tau}_3 \right) X_{13} X_{12} \\ &\quad + U_0 T_\pi^2(r_{12}) T_\pi^2(r_{13}) \\ &= A_{2\pi} 2 \left(\vec{\tau}_2 \cdot \vec{\tau}_3 + \frac{i}{4} \vec{\tau}_1 \cdot \vec{\tau}_2 \times \vec{\tau}_3 \right) X_{12} X_{13} \\ &\quad + A_{2\pi} 2 \left(\vec{\tau}_2 \cdot \vec{\tau}_3 - \frac{i}{4} \vec{\tau}_1 \cdot \vec{\tau}_2 \times \vec{\tau}_3 \right) X_{13} X_{12} \\ &\quad + \frac{U_0}{2} \left(T_\pi^2(r_{12}) T_\pi^2(r_{13}) + T_\pi^2(r_{13}) T_\pi^2(r_{12}) \right)\end{aligned}\tag{A2}$$

Because the T^2 operators commute with each other, we could choose the symmetrical form in the last line.

The aim is to find matrix elements with respect to our standard basis states [59]

$$|p q \alpha \rangle_i \equiv |p q (ls) j (\lambda \frac{1}{2}) J (j J) \mathcal{J} \mathcal{M} (t \frac{1}{2}) T M_T \rangle_i\tag{A3}$$

Here the magnitudes of the Jacobi momenta of the subsystem and the outer particle are p and q , respectively. The angular dependence is expanded in partial waves. Corresponding to p and q we introduce angular momenta l and λ . As indicated in Eq.(A3) the orbital angular momenta couple with the spin of the subsystem s and the outer particle $\frac{1}{2}$ to the total spin of the subsystem j and outer particle J . These angular momenta are combined to the total spin \mathcal{J} and its third component \mathcal{M} . The total isospin of the subsystem t couples with the isospin of the outer particle $\frac{1}{2}$ to T and its third component M_T . Because we will make use of several sets of Jacobi momenta, we append an index i which gives the number of the outer particle.

According to Eqs.(1) and (4) the operator $V_4^{(1)}$ acts on completely antisymmetric 3N states $|\chi \rangle = (1 + P) |\phi \rangle$ or $|\chi \rangle = (1 + P) G_0 T$. In the next paragraphs we would like to establish some consequences of this fact.

To that aim we introduce a short hand notation for our basis states:

$$|(jk)i \rangle \equiv |p q \alpha \rangle_i\tag{A4}$$

In contrast to Eq.(A3) this definition fixes the ordering within the subsystem. (ij) is understood to fix the momentum vector to $\vec{p} = \frac{1}{2}(\vec{k}_i - \vec{k}_j)$ and the spin and isospin coupling

within the subsystem to $(s_i s_j)s$ and $(t_i t_j)t$. In consequence we can distinguish $|(ij)k\rangle$ and $|(ji)k\rangle$ in this notation. In the partial wave decomposition there is a simple phase relation connecting both states

$$|(ij)k\rangle = (-)^{l+s+t} |(ji)k\rangle \equiv (-)^{(ij)} |(ji)k\rangle \quad (\text{A5})$$

Of course all sets of basis states are complete, therefore we can expand the incoming state in several ways

$$\begin{aligned} |\chi\rangle &= \int |(31)2\rangle \langle (31)2|\chi\rangle \\ &= \int |(12)3\rangle \langle (12)3|\chi\rangle \end{aligned} \quad (\text{A6})$$

Due to the total antisymmetry of $|\chi\rangle$, its matrix elements are equal

$$\langle (31)2|\chi\rangle = \langle (12)3|\chi\rangle = \langle (23)1|\chi\rangle \quad (\text{A7})$$

In consequence we can expand the different terms in Eq.(A2) on the right hand side in different Jacobi coordinates. Let us begin with the two U_0 terms in Eq.(A2):

$$\begin{aligned} M_3 &= \frac{1}{2} \langle (23)1|(12)3''\rangle \langle (12)3''|T_\pi^2(r_{12})|(12)3'''\rangle \\ &\quad \langle (12)3'''\rangle \langle (31)2''''\rangle \langle (31)2''''|T_\pi^2(r_{13})|(31)2'\rangle \\ &\quad + \frac{1}{2} \langle (23)1|(31)2''\rangle \langle (31)2''|T_\pi^2(r_{13})|(31)2'''\rangle \\ &\quad \langle (31)2'''\rangle \langle (12)3''''\rangle \langle (12)3''''|T_\pi^2(r_{12})|(12)3'\rangle \end{aligned} \quad (\text{A8})$$

In this equation we introduced several completeness relations and projected on two kinds of incoming states keeping in mind that one can add up the matrix elements because of the total antisymmetry of $|\chi\rangle$. In the way we inserted the completeness relations in Eq.(A8), the matrix elements of T_π^2 are evaluated in their natural coordinates. In this form the operator is diagonal in the quantum numbers and momenta of the outer particle and additionally it conserves the symmetry with respect to the interchange of the particles of the subsystem.

The matrix element $\langle (12)3|T_\pi^2(r_{12})|(12)3'\rangle$ depends on Jacobi coordinates and quantum numbers which single out the subsystem (12). By renumbering the particles one finds

$$\langle (12)3|T_\pi^2(r_{12})|(12)3'\rangle = \langle (31)2|T_\pi^2(r_{13})|(31)2'\rangle \quad (\text{A9})$$

Note that the matrix element on the right hand side depends on coordinates which differ from the ones on the left hand side. Though the matrix elements are equal, one has to keep in mind that the actual meaning of the momenta and quantum numbers is different on both sides.

In the same manner one can find an important relation between the cyclic and anti cyclic transformations

$$\langle (ij)k|(jk)i'\rangle = \langle (ik)j|(kj)i'\rangle = (-)^{(ik)} (-)^{(kj)'} \langle (ki)j|(jk)i'\rangle \quad (\text{A10})$$

We would like to emphasize that the transformation itself doesn't conserve the symmetry of the subsystem and therefore the completeness relation in '' and ''' states in Eq.(A8) have to

include also the unphysical symmetric states in the two-body subsystems. With the help of Eq.(A10) and renumbering the particles in the second part of Eq.(A8) one finds

$$\begin{aligned}
M_3 = & \frac{1}{2} \langle (23)1|(12)3'' \rangle \langle (12)3''|T_\pi^2(r_{12})|(12)3''' \rangle \\
& \langle (12)3'''|(31)2'''' \rangle \langle (31)2''''|T_\pi^2(r_{13})|(31)2' \rangle \\
& + \frac{1}{2} (-)^{(23)} (-)^{(12)''} (-)^{(12)''''} (-)^{(31)''''} \langle (23)1|(12)3'' \rangle \langle (12)3''|T_\pi^2(r_{12})|(12)3''' \rangle \\
& \langle (12)3'''|(31)2'''' \rangle \langle (31)2''''|T_\pi^2(r_{13})|(31)2' \rangle
\end{aligned} \tag{A11}$$

Because T_π^2 conserves the symmetry of the subsystem $(-)^{(12)''} = (-)^{(12)''''}$ and $(-)^{(31)''''} = (-)^{(31)'}$. Therefore Eq.(A11) reduces to

$$\begin{aligned}
M_3 = & \frac{1}{2} \left(1 + (-)^{(23)} (-)^{(31)'} \right) \langle (23)1|(12)3'' \rangle \langle (12)3''|T_\pi^2(r_{12})|(12)3''' \rangle \\
& \langle (12)3'''|(31)2'''' \rangle \langle (31)2''''|T_\pi^2(r_{13})|(31)2' \rangle
\end{aligned} \tag{A12}$$

The incoming state is antisymmetric in the subsystem (31) hence $(-)^{(31)'} = -1$. Therefore M_3 is zero for outgoing states which are symmetric in the subsystem (23) and equals twice the first part for the antisymmetric outgoing states. We restrict the outgoing states to antisymmetric ones. Then it is justified to write

$$\begin{aligned}
M_3 = & \langle (23)1|(12)3'' \rangle \langle (12)3''|T_\pi^2(r_{12})|(12)3''' \rangle \\
& \langle (12)3'''|(31)2'''' \rangle \langle (31)2''''|T_\pi^2(r_{13})|(31)2' \rangle
\end{aligned} \tag{A13}$$

We would like emphasize again that we restrict the outgoing, incoming and '''' states to physical, antisymmetric states in the subsystems. Due to the coordinate transformations, the '' and ''' sums are not restricted anymore to antisymmetric subsystem states and the completeness relations run over all symmetries.

Lets turn to the $A_{2\pi}$ parts now. In the same manner we define the matrix elements of the $A_{2\pi}$ parts

$$\begin{aligned}
\tilde{M}_3 = & \langle (23)1|(12)3'' \rangle \langle (12)3''|X_{12}|(12)3''' \rangle \\
& \langle (12)3'''|2 \left(\vec{\tau}_2 \cdot \vec{\tau}_3 + \frac{i}{4} \vec{\tau}_1 \cdot \vec{\tau}_2 \times \vec{\tau}_3 \right) |(31)2'''' \rangle \langle (31)2''''|X_{13}|(31)2' \rangle \\
& + \langle (23)1|(31)2'' \rangle \langle (31)2''|X_{13}|(31)2''' \rangle \\
& \langle (31)2'''|2 \left(\vec{\tau}_2 \cdot \vec{\tau}_3 - \frac{i}{4} \vec{\tau}_1 \cdot \vec{\tau}_2 \times \vec{\tau}_3 \right) |(12)3'''' \rangle \langle (12)3''''|X_{12}|(12)3' \rangle
\end{aligned} \tag{A14}$$

The isospin operators commute with the X_{ij} operators. We combined them with the inner transformation matrix. Because $\vec{\tau}_2 \cdot \vec{\tau}_3$ is symmetric with respect to the interchange of particle 2 and 3 and $\vec{\tau}_1 \cdot \vec{\tau}_2 \times \vec{\tau}_3$ is antisymmetric, the steps leading to Eq.(A10) can be repeated with the isospin matrix element. In addition there is a sign change for the antisymmetric part of the isospin operators.

$$\begin{aligned}
& \langle (12)3'''|2 \left(\vec{\tau}_2 \cdot \vec{\tau}_3 + \frac{i}{4} \vec{\tau}_1 \cdot \vec{\tau}_2 \times \vec{\tau}_3 \right) |(31)2'''' \rangle \\
& = (-)^{(31)''''} (-)^{(12)''''} \langle (31)2''''|2 \left(\vec{\tau}_2 \cdot \vec{\tau}_3 - \frac{i}{4} \vec{\tau}_1 \cdot \vec{\tau}_2 \times \vec{\tau}_3 \right) |(12)3'''' \rangle
\end{aligned} \tag{A15}$$

The symmetry of the X_{ij} 's leads to equal phases on both sides of their matrix elements: $(-)^{(31)''''} = (-)^{(31)'}$ and $(-)^{(12)''} = (-)^{(12)''''}$. The matrix element of the $A_{2\pi}$ parts reduces to

$$\begin{aligned} \tilde{M}_3 = & \left(1 + (-)^{(23)}(-)^{(31)'}\right) \langle (23)1|(12)3'' \rangle \langle (12)3''|X_{12}|(12)3''' \rangle \\ & \langle (12)3'''|2 \left(\vec{\tau}_2 \cdot \vec{\tau}_3 + \frac{i}{4} \vec{\tau}_1 \cdot \vec{\tau}_2 \times \vec{\tau}_3 \right) |(31)2'''' \rangle \langle (31)2''''|X_{13}|(31)2' \rangle \end{aligned} \quad (\text{A16})$$

and it is again justified to restrict the outgoing states to antisymmetric subsystems and write

$$\begin{aligned} \tilde{M}_3 = & 2 \langle (23)1|(12)3'' \rangle \langle (12)3''|X_{12}|(12)3''' \rangle \\ & \langle (12)3'''|2 \left(\vec{\tau}_2 \cdot \vec{\tau}_3 + \frac{i}{4} \vec{\tau}_1 \cdot \vec{\tau}_2 \times \vec{\tau}_3 \right) |(31)2'''' \rangle \langle (31)2''''|X_{13}|(31)2' \rangle \end{aligned} \quad (\text{A17})$$

It is standard to work out the two-body partial wave matrix elements for X_{ij} and T_π^2 in terms of Bessel transforms. Also the isospin and coordinate transformation matrix elements are standard and we refer to [48].

REFERENCES

- [1] R. Machleidt, K. Holinde, Ch. Elster, Phys. Rep. **149**, 1 (1987).
- [2] R. Machleidt, Adv. Nucl. Phys. **19**, 189 (1989).
- [3] V. G. J. Stoks, R. A. M. Klomp, C. P. F. Terheggen, J. J. de Swart, Phys. Rev. **C49**, 2950 (1994).
- [4] R. B. Wiringa, V. G. J. Stoks, R. Schiavilla, Phys. Rev. **C51**, 38 (1995).
- [5] R. Machleidt, F. Sammarruca, and Y. Song, Phys. Rev. **C53**, R1483 (1996).
- [6] R. Machleidt, nucl-th/0006014.
- [7] S. Weinberg, Phys. Lett. **B251**, 288 (1990); Nucl. Phys. **B363**, 3 (1991).
- [8] U. van Kolck, Phys. Rev. **C49**, 2932 (1994).
- [9] C. Ordoñez, L. Ray, U. van Kolck, Phys. Rev. **C53**, 2086 (1996).
- [10] T.-S. Park, K. Kubodera, D.-P. Min, M. Rho, Nucl. Phys. **A646**, 83 (1999).
- [11] N. Kaiser, R. Brockmann, W. Weise, Nucl. Phys. **A625**, 758 (1997)., 014001 (2000).
- [12] E. Epelbaum, W. Glöckle, U.-G. Meißner, Nucl. Phys. **A637**, 107 (1998).
- [13] E. Epelbaum, W. Glöckle, U.-G. Meißner, Nucl. Phys. **A671**, 295 (2000).
- [14] E. Epelbaum, H. Kamada, A. Nogga, H. Witała, W. Glöckle, U.-G. Meißner, nucl-th/0007057.
- [15] A. Nogga, H. Kamada, W. Glöckle, Phys. Rev. Lett. **85**, 944 (2000).
- [16] M. Viviani, Nucl. Phys. **A631**, 111c (1998).
- [17] J. Carlson, R. Schiavilla, Rev. of Mod. Phys. **70**, 743 (1998).
- [18] R. B. Wiringa, Steven C. Pieper, J. Carlson, V. R. Pandharipande, Phys. Rev. **C62**, 014001 (2000).
- [19] For a short review see M. R. Robilotta, Few Body Syst. **Suppl. 2**, 35 (1987).
- [20] V.R. Pandharipande, to be published in the proceedings of the 16th International Conference on "Few-body Problems in Physics", March 6-10, 2000, Taipei.
- [21] W. Glöckle, H. Witała, D. Hüber, H. Kamada and J. Golak, Phys. Rep. **274**, 107 (1996).
- [22] H. Sakai, K. Sekiguchi, H. Witała, W. Glöckle, M. Hatano, H. Kamada, H. Kato, Y. Maeda, A. Nogga, T. Ohnishi, H. Okamura, N. Sakamoto, S. Sakoda, Y. Satou, K. Suda, A. Tamii, T. Uesaka, T. Wakasa, and K. Yako, Phys. Rev. Lett. **84**, 5288 (2000); H. Sakai *et al.*, to be published in the proceedings of the 16th International Conference on "Few-body Problems in Physics", March 6-10, 2000, Taipei.
- [23] N. Sakamoto *et al.*, Phys. Lett. **B367**, 60 (1996).
- [24] W. Tornow, C.R. Howell, R.C. Byrd, R.S. Pedroni, and R.L. Walter, Phys. Rev. Lett. **49**, 312 (1982).
- [25] H.O. Meyer, Nucl. Phys. **A631**, 122c (1998).
- [26] R. V. Cadman *et al.*, submitted for publication.
- [27] R. Bieber *et al.*, Phys. Rev. Lett. **84**, 606 (2000).
- [28] P. Hempen *et al.*, Phys. Rev. **C57**, 484 (1998).
- [29] W. Grüebler, Nucl. Phys. **A353**, 31c (1981).
- [30] L. Sydow *et al.*, Nucl. Phys. **A567**, 55 (1994); L. Sydow *et al.*, Few-Body Syst. **25**, 133 (1998).
- [31] B. S. Pudliner, V. R. Pandharipande, J. Carlson, Steven C. Pieper, and R. B. Wiringa, Phys. Rev. **C56**, 1720 (1997).
- [32] D. Hüber, H. Kamada, H. Witała, and W. Glöckle, Acta Physica Polonica **B28**, 1677 (1997).

- [33] A. Stadler, W. Glöckle, P. U. Sauer, Phys. Rev. **C44**, 2319 (1991).
- [34] D. Hüber, H. Witała, W. Glöckle, Few Body Syst. **14**, 171 (1993).
- [35] G. O. Ohlsen, Rep. Prog. Phys. **35**, 717 (1972).
- [36] S. A. Coon, W. Glöckle, Phys. Rev. **C23**, 1970 (1981).
- [37] A. Nogga, D. Hüber, H. Kamada, W. Glöckle, Phys. Lett. **B409**, 19 (1997).
- [38] S. A. Coon, M. T. Peña, Phys. Rev. **C48**, 2559 (1993).
- [39] S. A. Coon, M. T. Peña, D. O. Riska, Phys. Rev. **C52**, 2925 (1995).
- [40] B. D. Keister, R. B. Wiringa, Phys. Lett. **B173**, 5 (1986).
- [41] T.-Y. Saito, J. Haidenbauer, nucl-th/0003064.
- [42] J. L. Friar, D. Hüber, U. van Kolck, Phys. Rev. **C59**, 53 (1999).
- [43] D. Hüber, J. L. Friar, A. Nogga, H. Witała, U. van Kolck, nucl-th/9910034.
- [44] M. R. Robilotta, H. T. Coelho, Nucl. Phys. **A460**, 645 (1986).
- [45] A. Kievsky, M. Viviani, S. Rosati, Phys. Rev. **C52**, R15 (1995).
- [46] A. Kievsky, S. Rosati, W. Tornow, M. Viviani, Nucl. Phys. **A607**, 402 (1996).
- [47] J. Fujita, H. Miyazawa, Prog. Theor. Phys. **17**, 360 (1957).
- [48] D. Hüber, H. Witała, A. Nogga, W. Glöckle, H. Kamada, Few Body Syst. **22**, 107 (1997).
- [49] H. Witała, W. Glöckle, J. Golak, D. Hüber, H. Kamada, A. Nogga, Phys. Lett. **B447**, 216 (1999).
- [50] P. U. Sauer, Prog. Part. Nucl. Phys. **16**, 35 (1986).
- [51] S. Nemoto *et al.*, Phys. Rev. **C58**, 2599 (1999).
- [52] H. Witała, W. Glöckle, D. Hüber, J. Golak, H. Kamada, Phys. Rev. Lett. **81**, 1183 (1998).
- [53] E. J. Stephenson, H. Witała, W. Glöckle, H. Kamada, A. Nogga, Phys. Rev. **C60**, 061001 (1999).
- [54] J.E. McAninch *et al.*, Phys. Lett. **B 307**, 13 (1993).
- [55] A. Kievsky, M. Viviani, and S. Rosati, Nucl. Phys. **A577**, 511 (1994).
- [56] H. Witała, D. Hüber, W. Glöckle, Phys. Rev. **C49**, R14 (1994).
- [57] W. Tornow, H. Witała, Nucl. Phys. **A637**, 280 (1998).
- [58] A. Kievsky, Phys. Rev. **C60**, 034001 (1999).
- [59] W. Glöckle, *The Quantum Mechanical Few-Body Problem*, Springer-Verlag, Berlin, 1983.
- [60] K. Sagara *et al.*, Phys. Rev. **C50**, 576 (1994).
- [61] S. Shimizu *et al.*, Phys. Rev. **C52**, 1193 (1995).
- [62] H. Rühl *et al.*, Nucl. Phys. **A524**, 377 (1991).
- [63] G. Igo *et al.*, Nucl. Phys. **A195**, 33 (1972).
- [64] H. Postma and R. Wilson, Phys. Rev. **121**, 1129 (1961).
- [65] K. Kuroda, A. Michałowicz, and M. Poulet, Nucl. Phys. **88**, 33 (1966).
- [66] R.E. Adelberger and C.N. Brown, Phys. Rev. **D5**, 2139 (1972).
- [67] S.P. Wells *et al.*, Nucl. Instrum. Methods Phys. Res., Sect. **A325**, 205 (1993).
- [68] H. Witała *et al.*, Few-Body Syst. **C15**, 67 (1993).

TABLES

	$\Lambda [m_\pi]$
CD Bonn+TM	4.856
AV18+TM	5.215
Nijm I+TM	5.120
Nijm II+TM	5.072
Nijm'93+TM	5.212

TABLE I. The cut-off parameters Λ from Eq. (7) used in the given potential combinations.

FIGURES

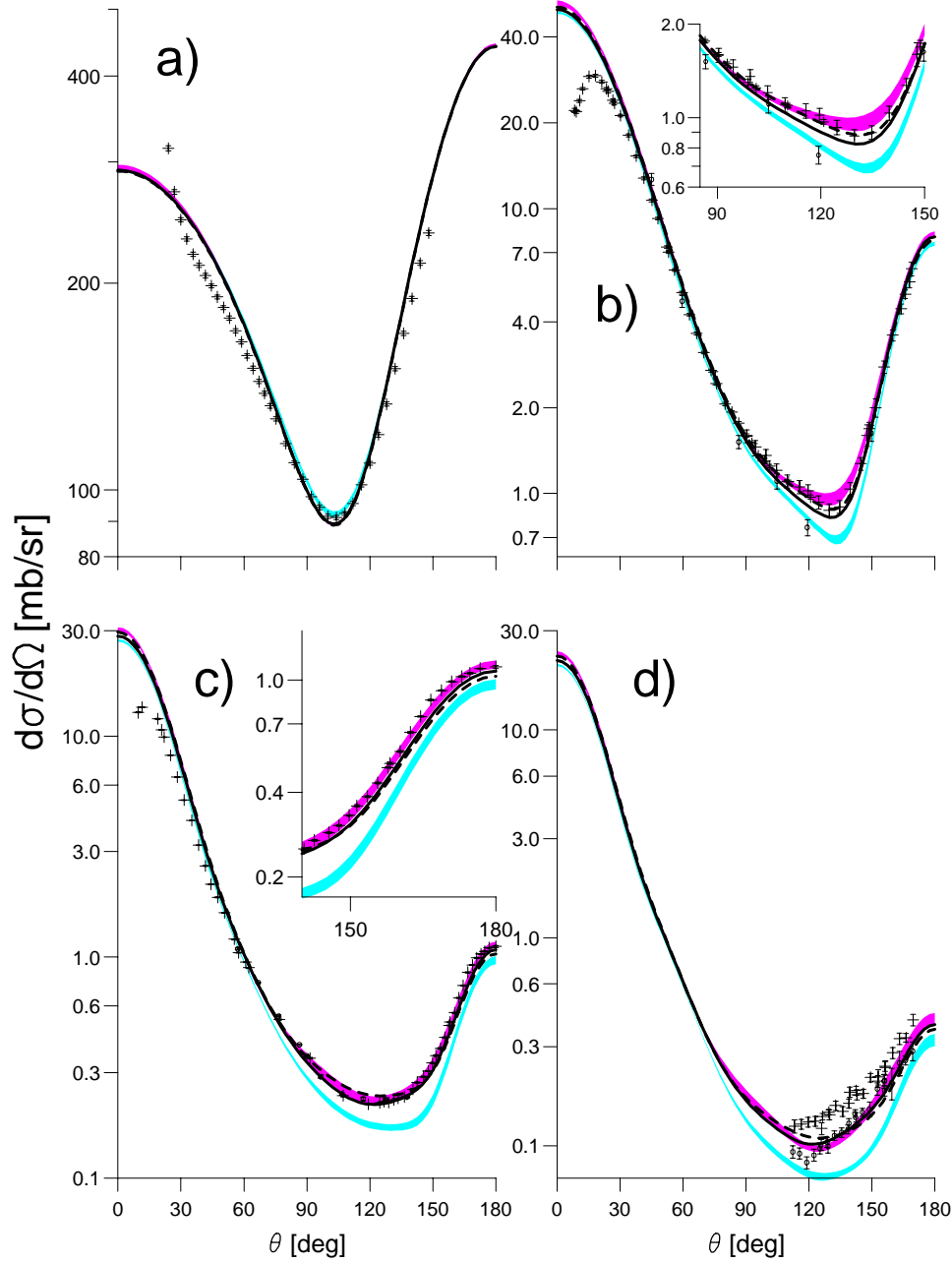


FIG. 1. The differential cross section in elastic Nd scattering at 3 (a), 65 (b), 135 (c) and 190 MeV (d). Two bands are shown in each subfigure, the light shaded one contains NN force predictions, the darker shaded one the NN force predictions+TM 3NF. The solid curves are the AV18+URBANA IX predictions. The dashed curves are the CD Bonn+TM' predictions. Data at 3 MeV from [60] (pd), at 65 MeV from [61] (pd-crosses) and [62] (nd-circles), at 135 MeV from [22] (pd-crosses), [23] (pd-circles), and at 190 MeV from [63] (pd: crosses 181 MeV, circles 216.5 MeV). In some cases error bars are not visible on the scale of the figure.

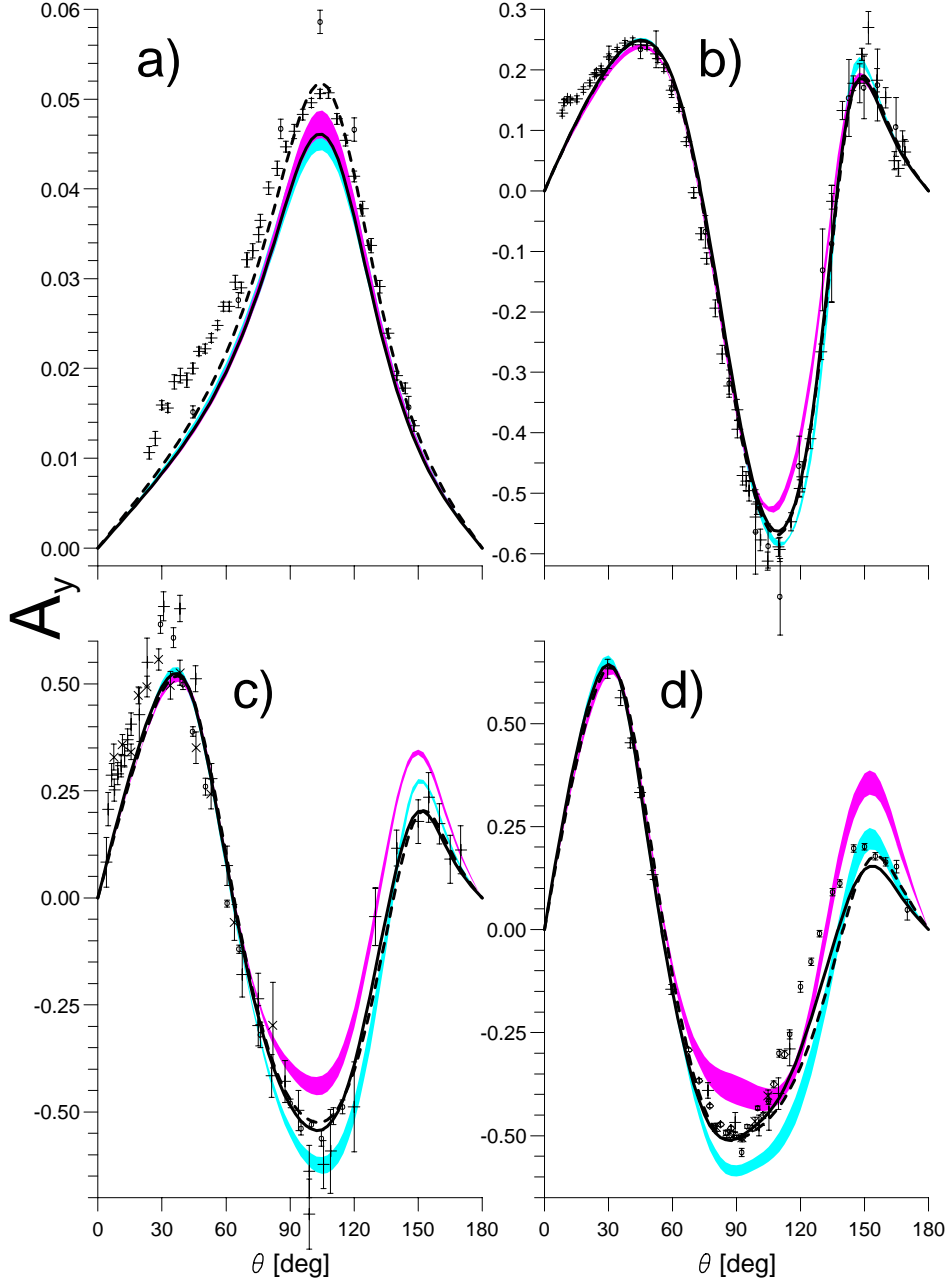


FIG. 2. The analyzing power $A_y(N)$ for elastic Nd scattering. Curves and the sequence of energies as in Fig. 1. Data at 3 MeV from [61] (pd-crosses) and [54] (nd-circles), at 65 MeV from [61] (pd-crosses) and [62] (nd-circles), at 135 MeV from [27] (pd-circles 150 MeV), [64] (pd-crosses 146 MeV), [65] (pd-x's 155 MeV), and at 190 MeV from [27] (pd-crosses 190 MeV), [66] (pd-circles 198 MeV), [67] (pd-squares 197 MeV).

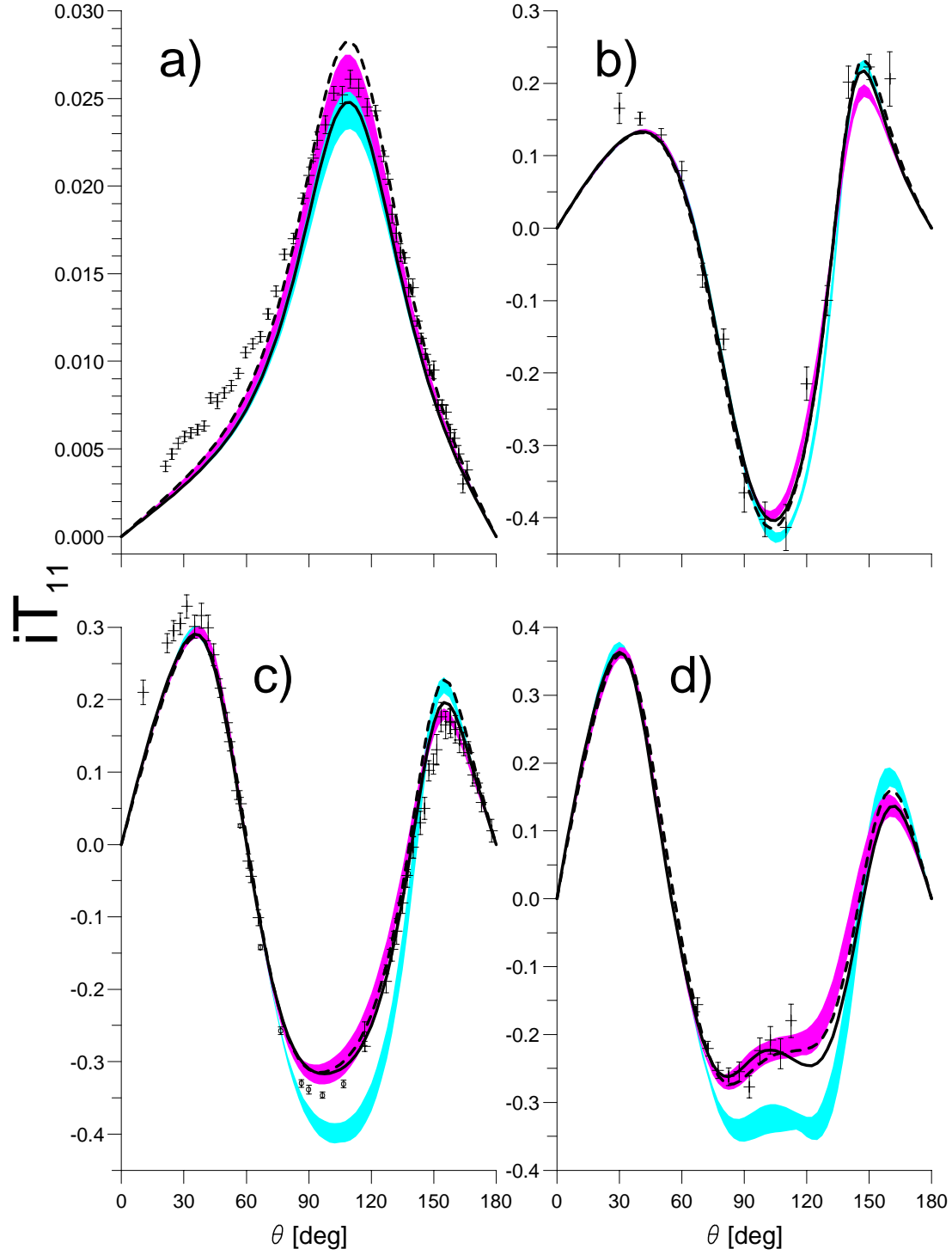


FIG. 3. The deuteron vector analyzing power iT_{11} for elastic Nd scattering. Curves and the sequence of energies as in Fig. 1. pd data at 3 MeV from [61], at 65 MeV from [68], at 135 MeV from [22] (crosses), [23] (circles), and at 190 MeV from [26].

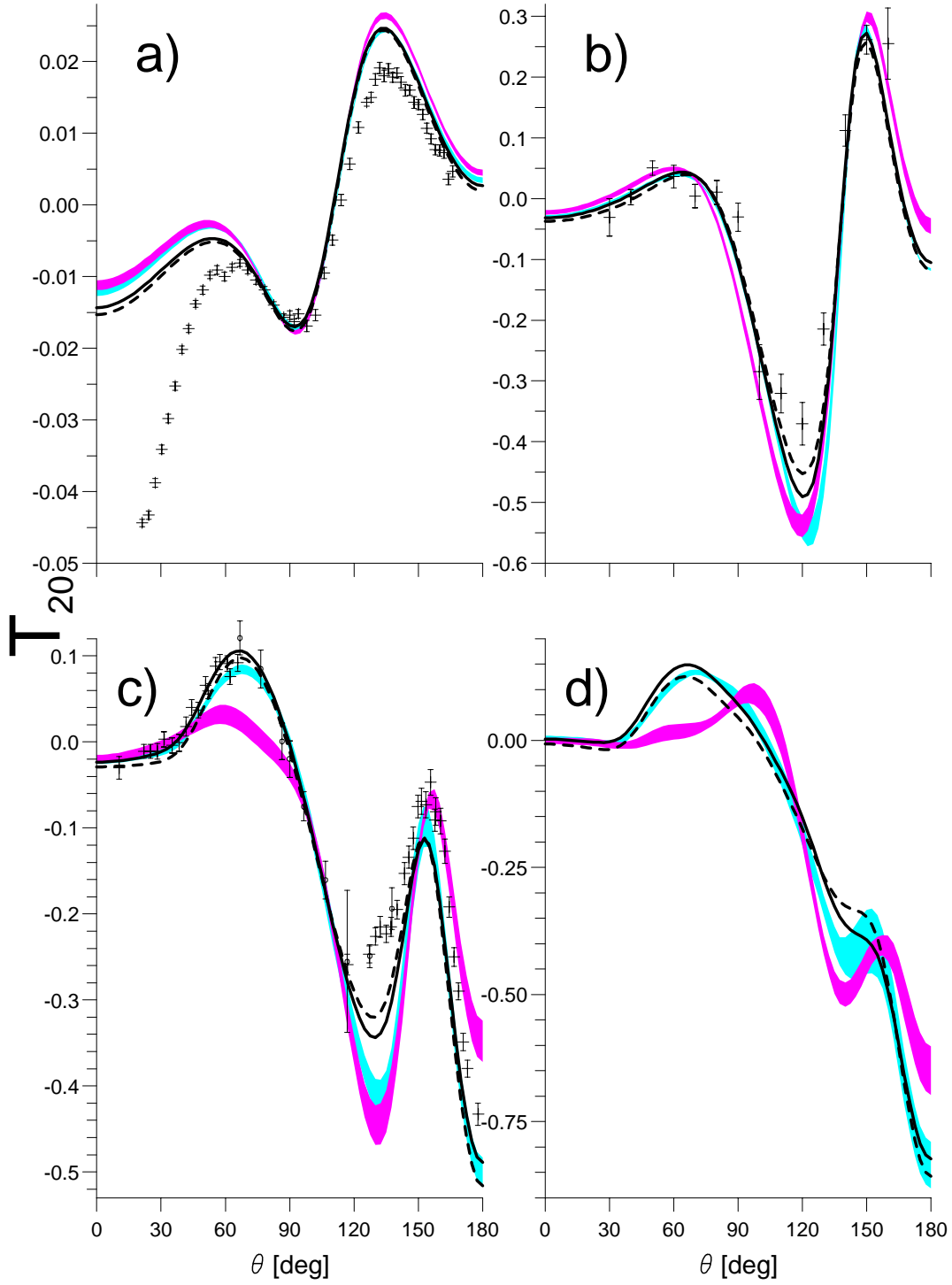


FIG. 4. The tensor analyzing power T_{20} for elastic Nd scattering. Curves and the sequence of energies as in Fig. 1. pd data at 3 MeV from [61], at 65 MeV from [68], and at 135 MeV from [22] (crosses), [23] (circles).

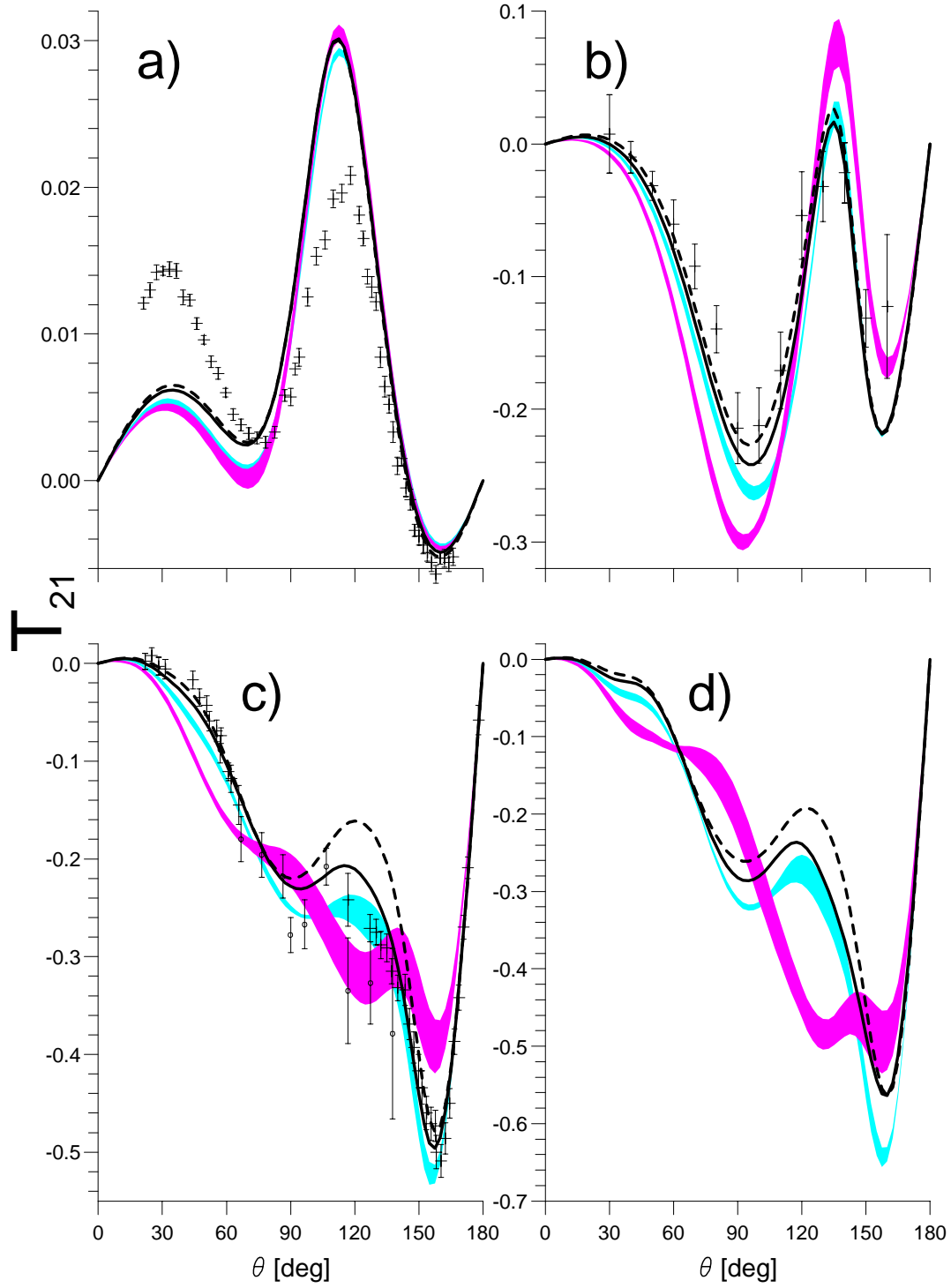


FIG. 5. The tensor analyzing power T_{21} for elastic Nd scattering. Curves and the sequence of energies as in Fig. 1. pd data at 3 MeV from [61], at 65 MeV from [68], and at 135 MeV from [22] (crosses), [23] (circles).

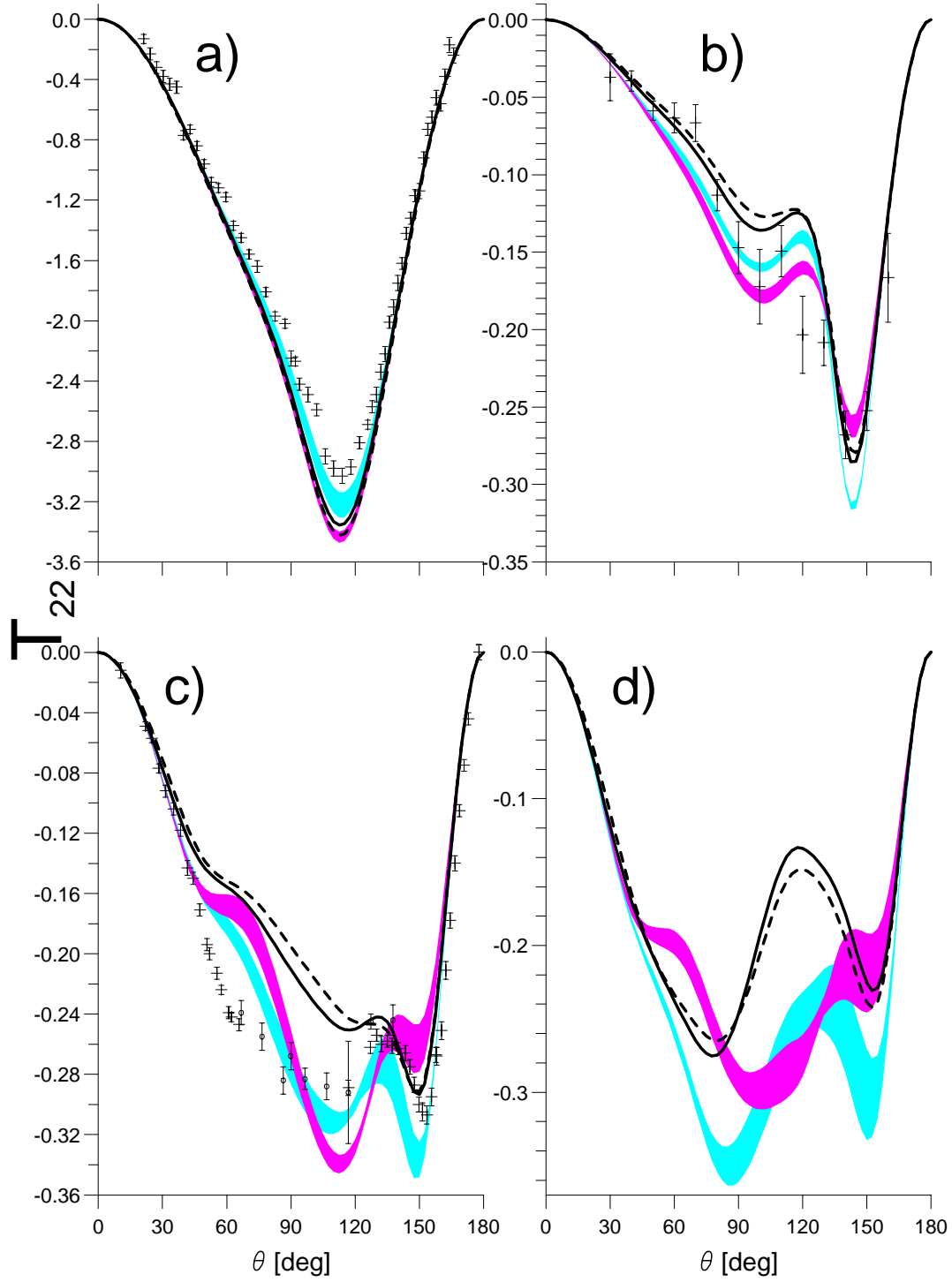


FIG. 6. The tensor analyzing power T_{22} for elastic Nd scattering. Curves and the sequence of energies as in Fig. 1. pd data at 3 MeV from [61], at 65 MeV from [68], and at 135 MeV from [22] (crosses), [23] (circles).

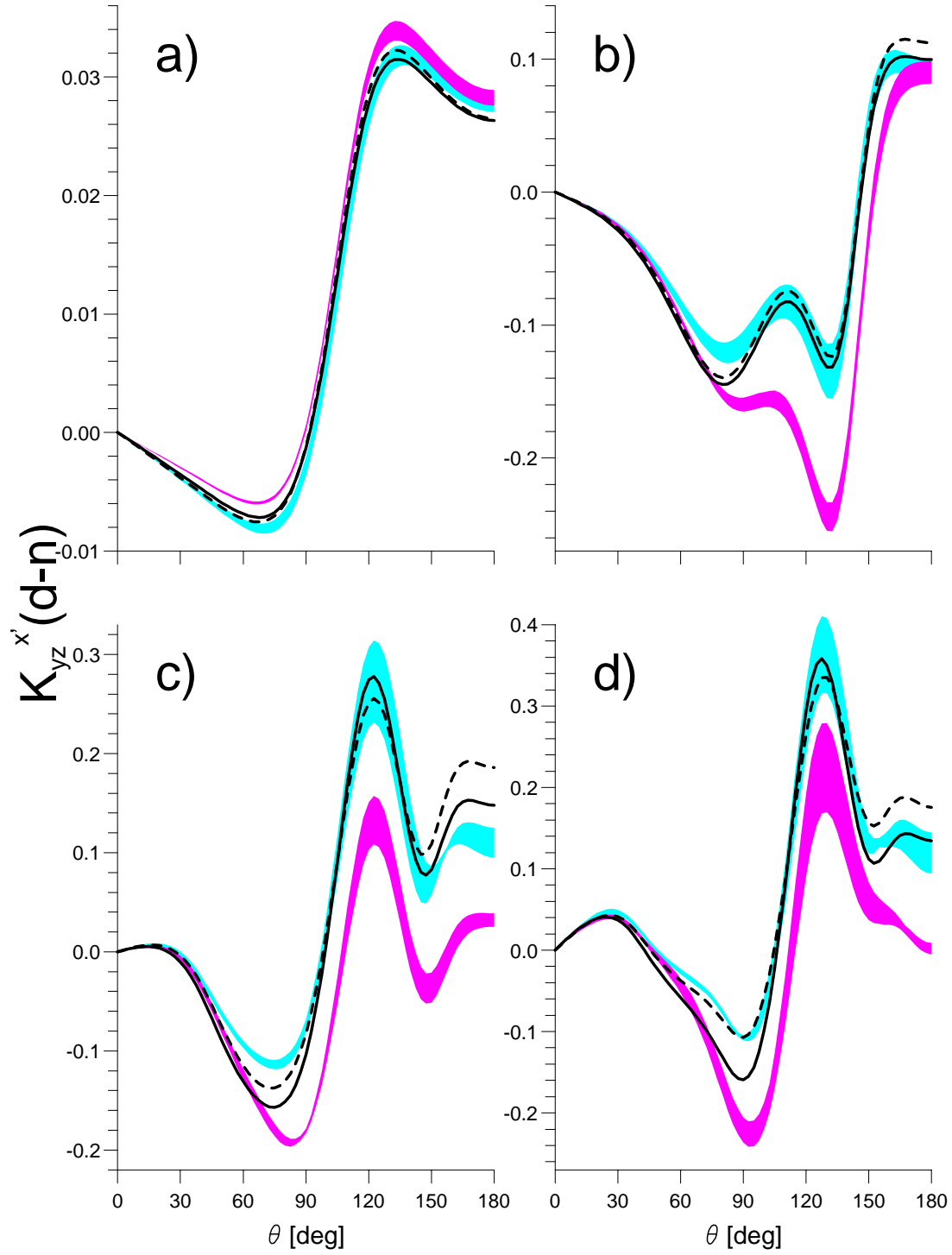


FIG. 7. The spin transfer coefficient $K_{yz}^{x'}$ for elastic Nd scattering. Curves and the sequence of energies as in Fig. 1.

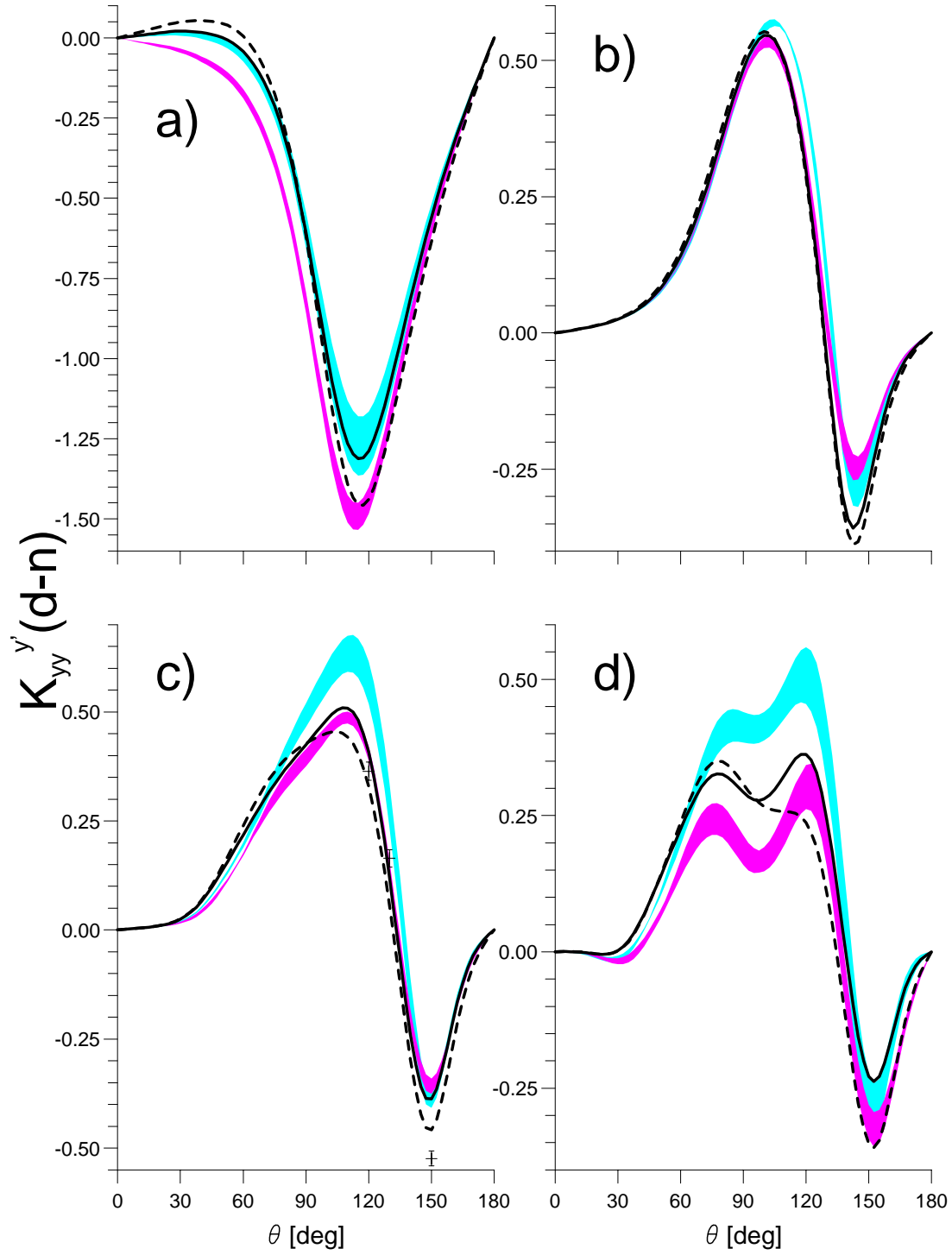


FIG. 8. The spin transfer coefficient $K_{yy}^{y'}$ for elastic Nd scattering. Curves and the sequence of energies as in Fig. 1. pd data at 135 MeV from [22].

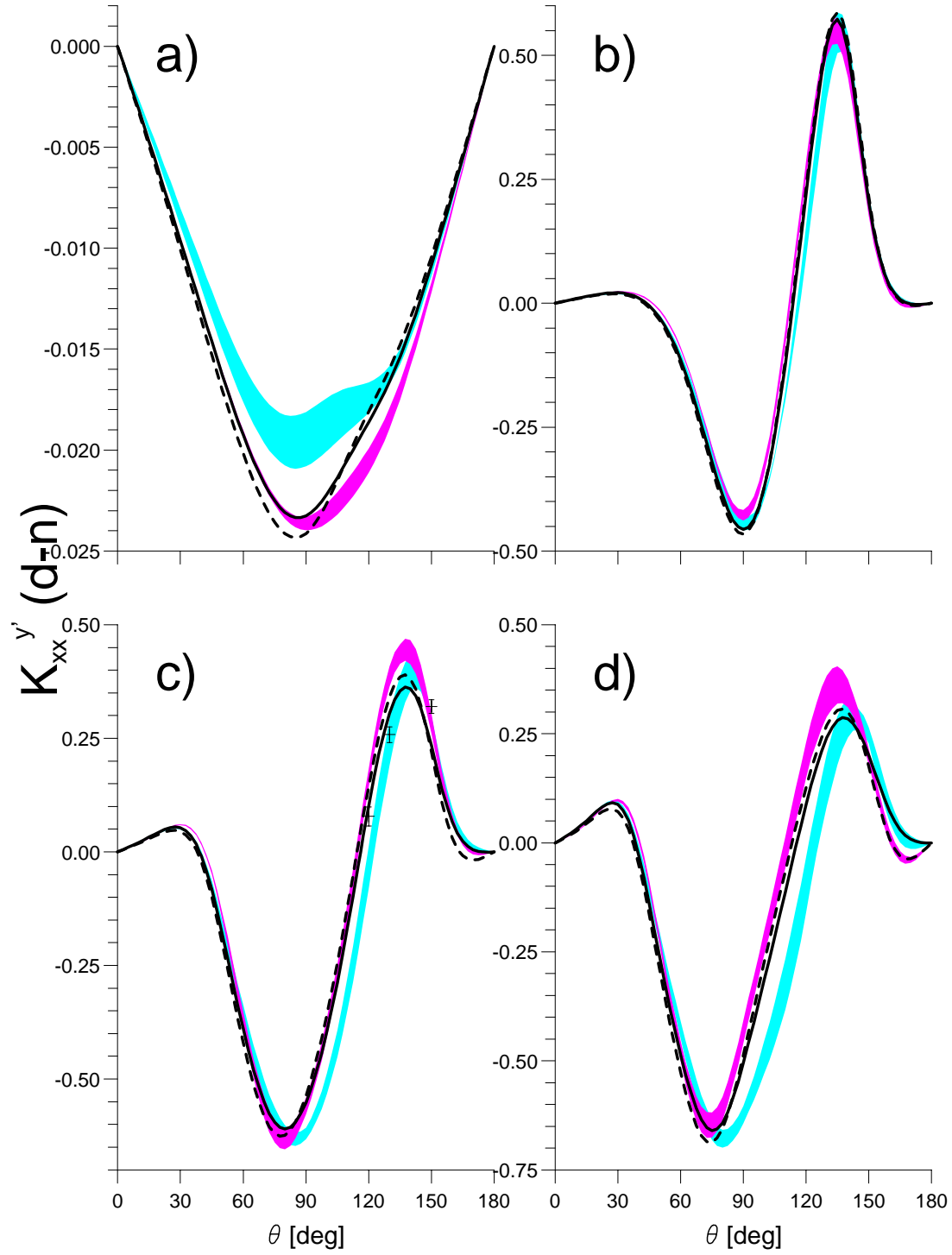


FIG. 9. The spin transfer coefficient K_{xx}^y for elastic Nd scattering. Curves and the sequence of energies as in Fig. 1. pd data at 135 MeV from [22].

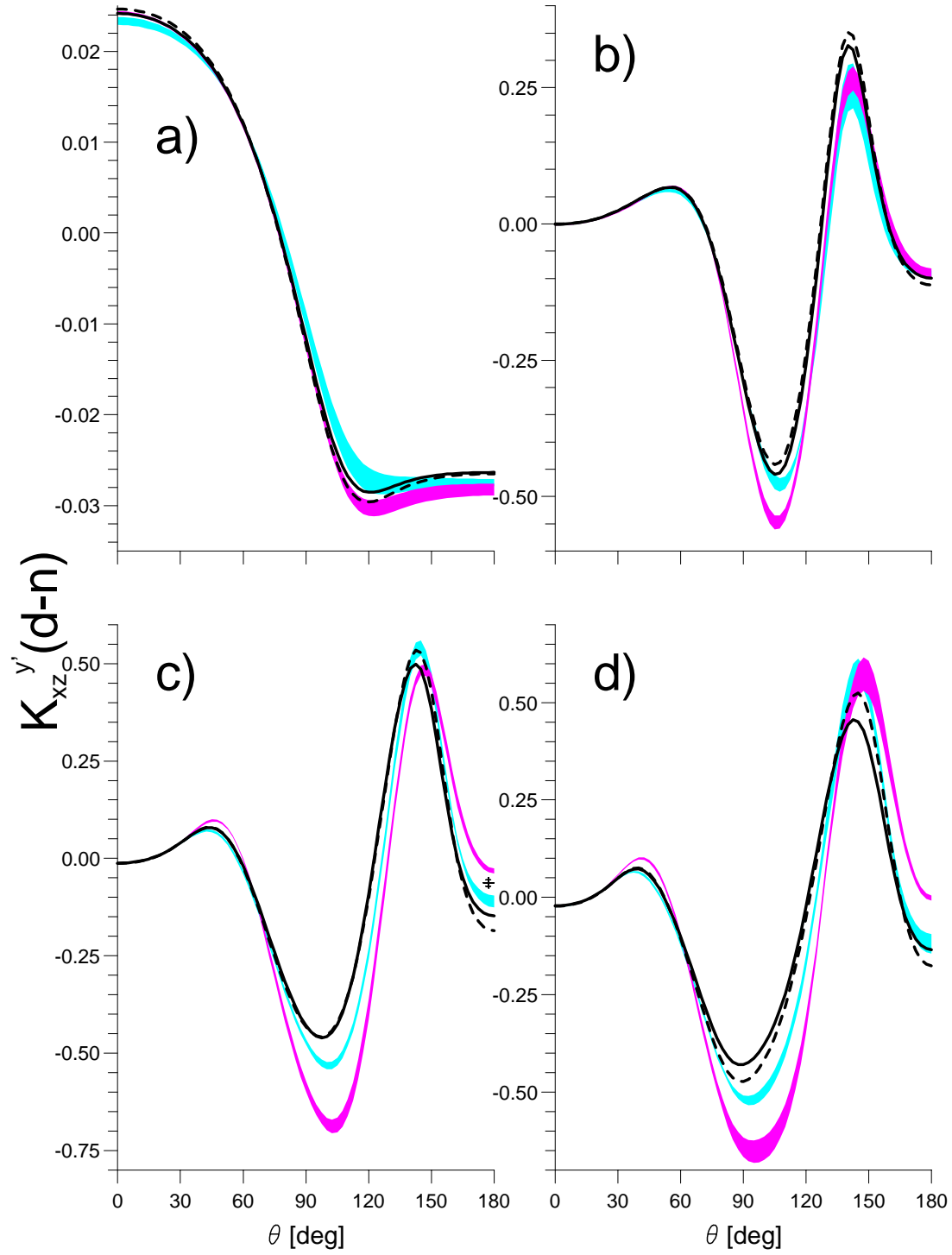


FIG. 10. The spin transfer coefficient $K_{xz}^{y'}$ for elastic Nd scattering. Curves and the sequence of energies as in Fig. 1. pd data at 135 MeV from [22].

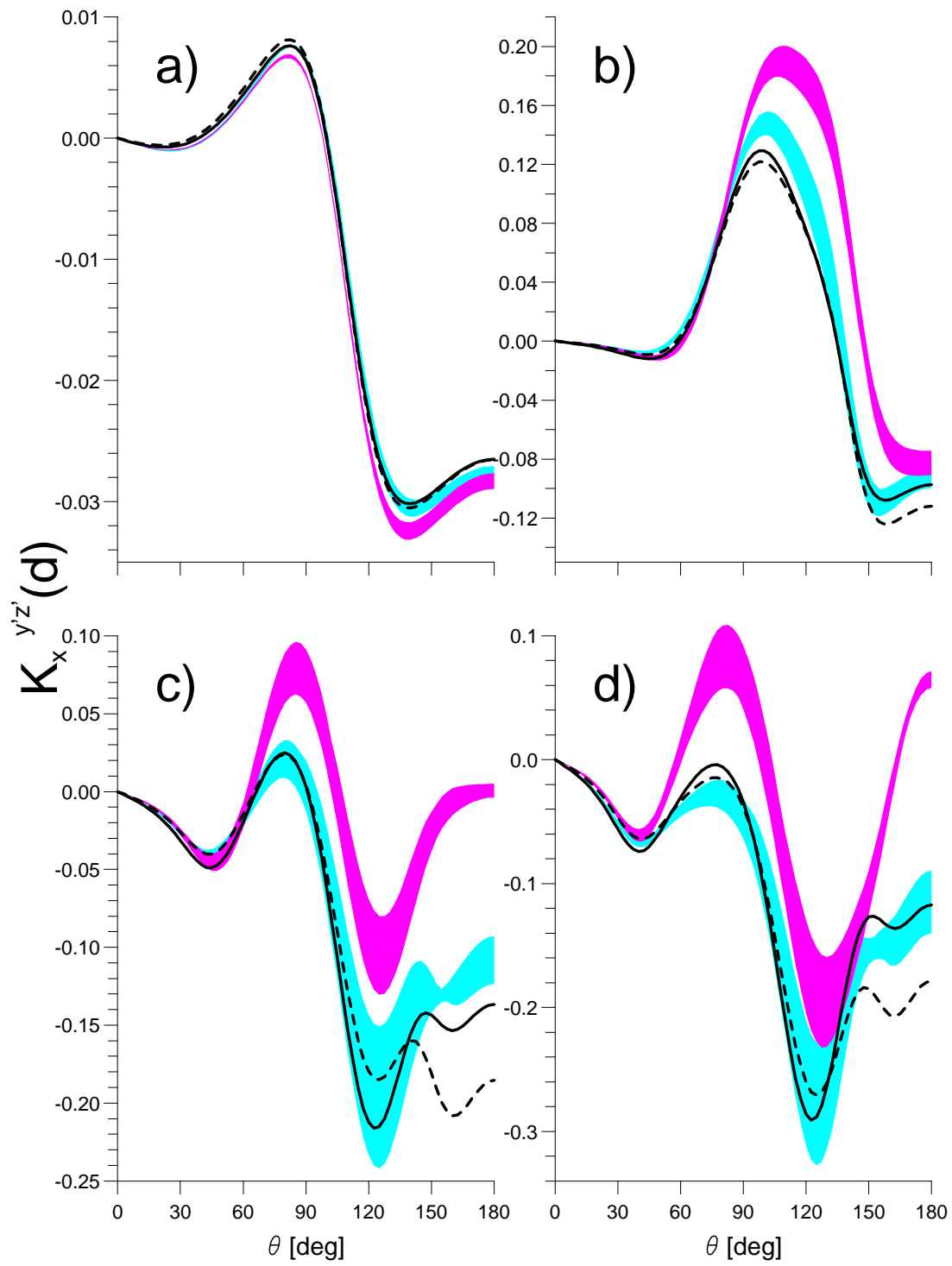


FIG. 11. The spin transfer coefficient $K_x^{y'z'}$ for elastic Nd scattering. Curves and the sequence of energies as in Fig. 1.

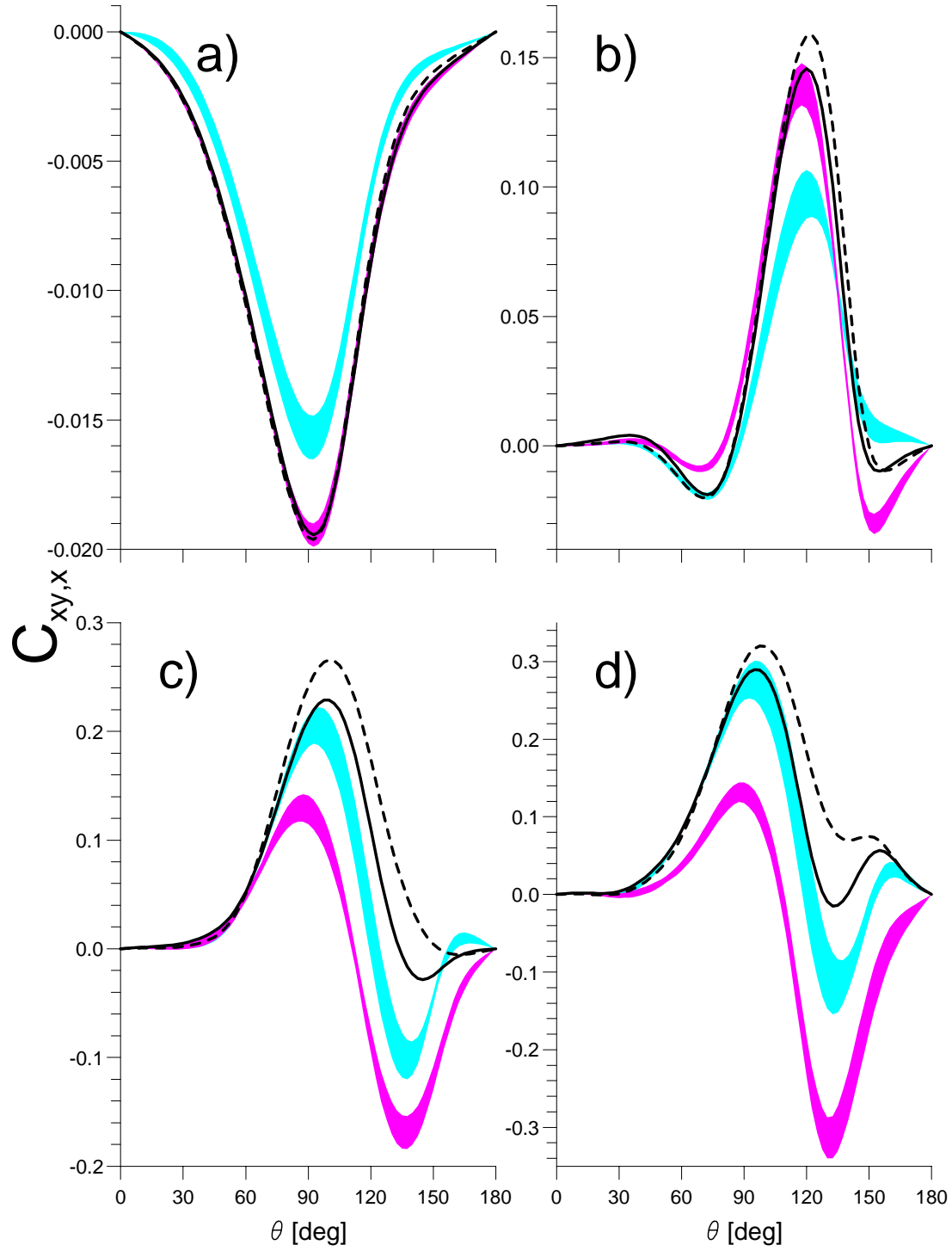


FIG. 12. The spin correlation coefficient $C_{xy,x}$ for elastic Nd scattering. Curves and the sequence of energies as in Fig. 1.

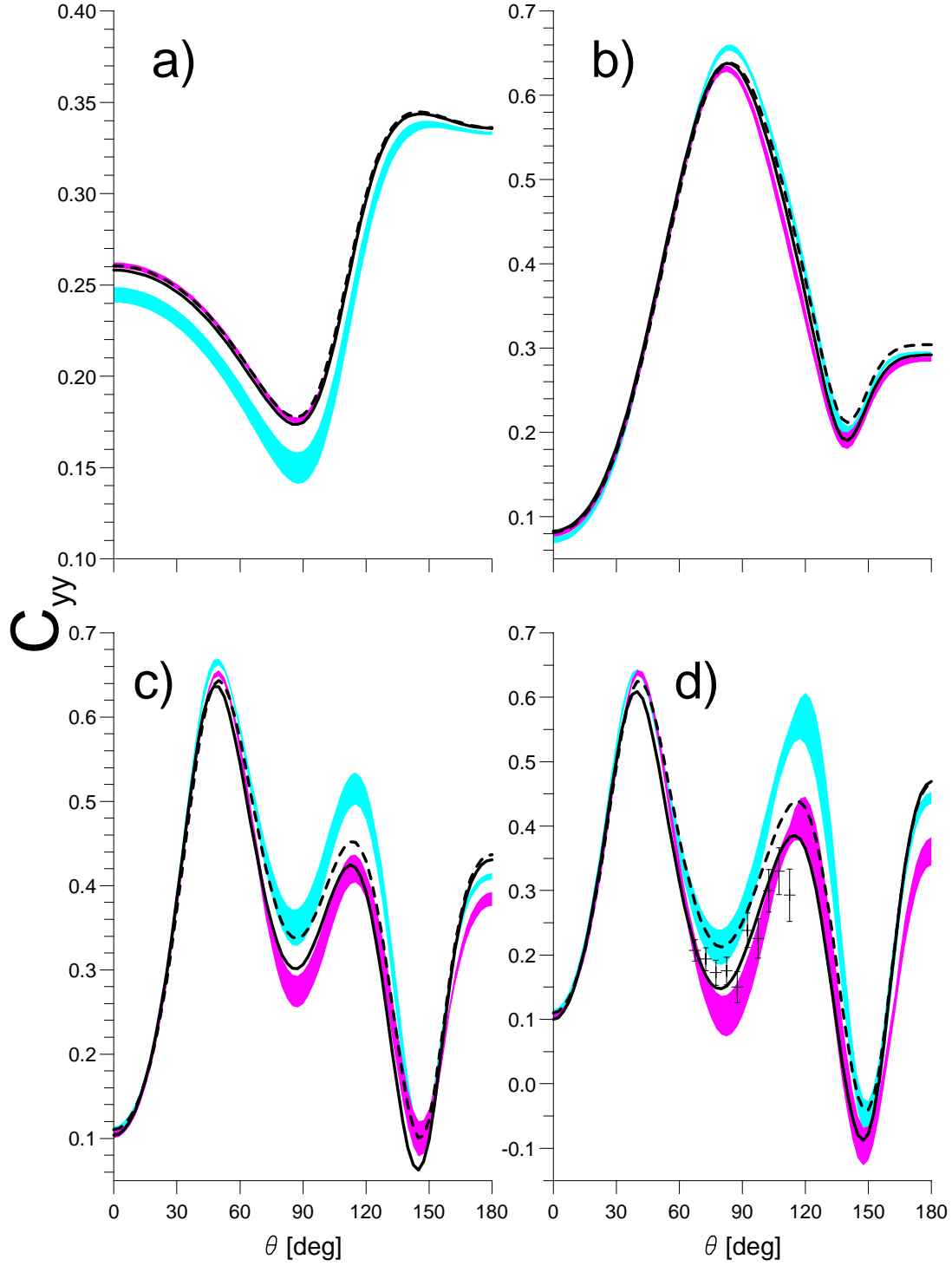


FIG. 13. The spin correlation coefficient C_{yy} for elastic Nd scattering. Curves and the sequence of energies as in Fig. 1. pd data at 190 MeV from [26].

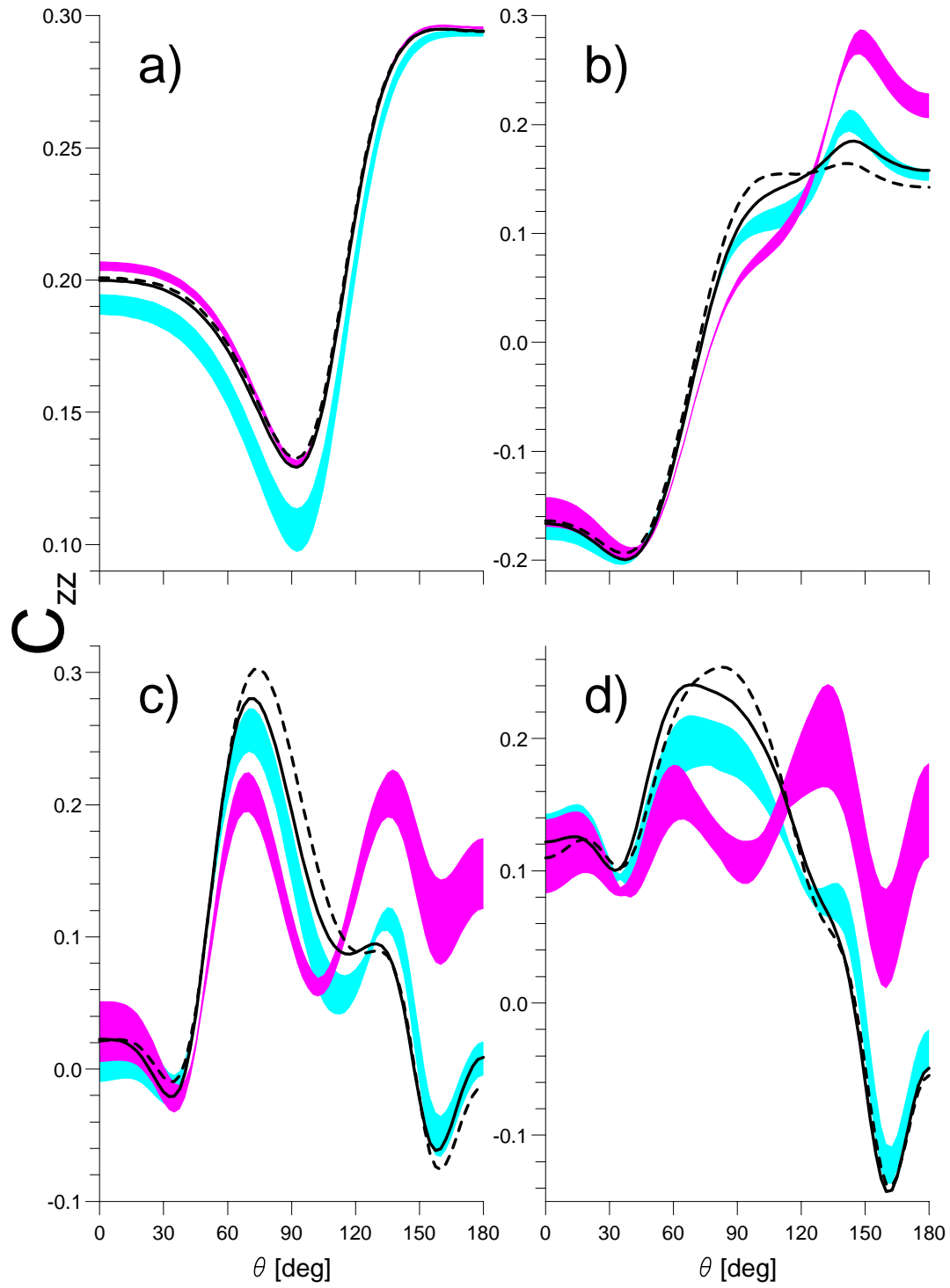


FIG. 14. The spin correlation coefficient C_{zz} for elastic Nd scattering. Curves and the sequence of energies as in Fig. 1.